YMTHE, Volume *27*

Supplemental Information

Suppression of Zika Virus Infection in the Brain by the Antiretroviral Drug Rilpivirine

Ilker Kudret Sariyer, Jennifer Gordon, Tricia H. Burdo, Hassen S. Wollebo, Eleonora Gianti, Martina Donadoni, Anna Bellizzi, Stephanie Cicalese, Regina Loomis, Jake A. Robinson, Vincenzo Carnevale, Joseph Steiner, Mehmet H. Ozdener, Andrew D. Miller, Shohreh Amini, Michael L. Klein, and Kamel Khalili

MATERIALS AND METHODS

Cell lines and culture. Primary human fetal astrocytes (PHFA), neurons (PHFN), and microglia (PHFM) were obtained from Comprehensive NeuroAIDS Center (CNAC) tissue culture core at Temple University Lewis Katz Medical School. hNPCs (H9-derived) were purchased from Gibco and maintained in neurobasal medium supplemented with 1% B-27, 1% glutamax, and 1% gentamycin. Astrocytes were maintained in DMEM/F12 (Gibco, Thermofisher Scientific), containing 15% FBS, 0.1% Gentamycin, and 0.1% insulin from bovine (Sigma). Microglia were maintained in DMEM/F12 (Gibco, Thermofisher Scientific), containing 10% FBS, 0.1% Gentamycin, D-Biotin (0.1 µg/ml), and 0.1% insulin from bovine (Sigma). Neurons were seeded into poly-D-lysine coated plates and kept in neurobasal medium containing1% glutamax, 1% B-27 supplement, 0.1% gentamycin, and 0.1% amphotericin B. Half of the neuronal growth medium was replaced with fresh medium every 3 to 4 days.

ZIKV strains and propagation. ZIKV strain PRVABC59 is isolated from a patient isolate in Puerto Rico in 2015, that was obtained from ATCC (VR-1843) and propagated in Vero cells for further production and purification. Culture supernatants from Vero cells infected with ZIKV were collected at 4 dpi and centrifuged at 3,000 RPM for 15 minutes to remove cell debris. ZIKV particles were concentrated by ultracentrifugation of the clarified media for 4 hours at 23,600 RPM at 4 °C. Media was aspirated, and viral particles re-suspended in 1 mL PBS. Virus was further purified utilizing an Optiprep discontinuous 20/55% gradient and ultracentrifugation. Optiprep, a 60% iodixanol solution was diluted into a 20% and 55% layer, 16 mL each, with 20% layered on top of the 55% solution. Viral particles were harvested from the gradient interface and kept frozen at -80 °C or used for plaque-forming assay for infectivity quantification.

Plaque-forming assay. Vero cells were seeded in 6 well plates at a concentration of 1 X 10^6 cells/well 48 hours prior to inoculation and grown in DMEM containing 5% FBS and 1% penicillin/streptomycin. On day of infection, serial dilutions of ZIKV infected culture medium were made by diluting 100 uL media in 900 uL OptiMEM from 10^{-2} to 10^{-6} dilutions. 900 uL of each viral

dilution was added to confluent vero cells and inoculated at 37 °C for 2 hours. Inoculum was aspirated and fresh DMEM was added and changed every two days. On day five post-infection, vero cells were fixed in 10%

formaldehyde in PBS and stained with a 0.1% solution of crystal violet in 70% methanol, and the virus titers were calculated by scoring the plaque-forming units (PFU).

ZIKV infection in primary human CNS cells. To investigate ZIKV propagation in the CNS cells, PHFA, PHFM, PHFN, PHAA, and hNPCs (H9) cells were seeded into 6-well plates and infected with ZIKV (0.1 PFU). Cells were seeded at a density of 1 x 10^6, grown to confluency and inoculated with 1 mL OptiMEM containing diluted virus. Cells were incubated for 2 hours at 37 °C, before media was exchanged for fresh media. Media was collected from infected cells at various time points of post-infections, centrifuged at 3,000 RPM for 15 minutes to remove cell debris, and used in real time qRT-PCR for analysis of shed viral particles. Whole cell lysates and RNA samples were also collected from the cells. Protein lysates were collected by lysing cells in 1X TNN buffer with protease inhibitor cocktail (Sigma), rotating for 30 minutes, followed by centrifugation to collect supernatant. RNA was purified via Trizol Reagent protocol (Invitrogen, Thermofisher Scientific). Whole cell lysates were used for Western blot analysis of viral proteins. Cell RNA was either analyzed for viral RNA copies via real time qRT-PCR or by RT-PCR for viral genes.

Real time qRT-PCR. Either 10 uL media from infected cells or 20 ng cell RNA or tissue RNA was used for real time qRT-PCR analysis of ZIKV copies as described by Lanciotti et al.[1]. All real-time assays were performed by using the QuantiTect Probe RT-PCR kit (QIAGEN, Valencia, CA, USA) with amplifications in the LightCycler 96 instrument (Roche, Indianapolis, IN, USA). The standard curve was generated using a ZIKV with known copies (3.2 x 10^7 viral copies/mL) and diluted 10 folds. Ct values for each sample were converted to viral copies/ml using the following equation:

$$Quantity = 10^{\frac{Ct-b}{m}}$$

Where quantity is ZIKV copies/ml, Ct is the threshold cycle at which the fluorescence value for the sample was significantly higher than background, b is the y intercept of the standard curve, and m is the slope of the standard curve. The following ZIKV specific primers were used in the reactions:

ZIKV-1086 (1086–1102) CCGCTGCCCAACACAAG,

ZIKV-1162c (1162–1139) CCACTAACGTTCTTTTGCAGACAT,

ZIKV-1107-FAM (1107–1137) AGCCTACCTTGACAAGCAGTCAGACACTCAA-6FAM.

Western blot analysis. Whole-cell extracts (WCE) were prepared from cells after washing with PBS by lysingwith TNN lysis buffer (40 mM Tris-HCL pH 7.4, 150 mM NaCl, 1 mM DTT, 1 mM EDTA, 1% NP40, and 1% protease inhibitors cocktail). Protein extracts were eluted with Laemmli sample buffer, heated at 95 °C for 10 min, resolved by SDS—PAGE and transferred to reinforced supported nitrocellulose membranes (Whatman, Germany) for 2 h at 4 °C in a transfer buffer containing 25 mM Tris (pH 7.4), 200 mM glycine, and 20% methanol. Membranes were blocked for 1 h at room temperature with 10% nonfat dry milk in PBS with 0.1% Tween-20 (PBST), washed and incubated with primary antibodies overnight in 5% nonfat dry milk at 4 °C. The blots were subsequently washed three times and incubated with IRDye 800CW goat anti-mouse and IRDye 680RD goat anti-rabbit secondary antibodies and visualized with an Odyssey CLx Imaging System (LI-COR, Inc.,). The following antibodies were used for Western blot: Zika Capsid antibody (GeneTex, cat#GTX133304), β Actin, and GAPDH.

MTT cell viability assay

Primary human fetal astrocytes were cultured in 12-well tissue culture plates and treated in triplicate with different concentrations of RPV (0, 1, 5, 10, 25, and 50 uM) based on previous studies in culture conditions[4,5] for 48 hours. After treatments, cells were incubated for 2 hours at 37°C with 150 µl of MTT (3-(4 5-dimethylthiazol-2-yl)-2 5-diphenyltetrazolium bromide) at 0.5 mg/ml working solution. The converted insoluble purple formazan was solubilized with 500 µl of

acidic isopropanol (0.004 M HCl in isopropanol). Absorbance of the converted formazan was measured at a wavelength of 570 nm with a background subtraction at 650 nm.

NNRTIs treatment of primary human CNS cells for ZIKV replication inhibition. The following HIV non-nucleoside reverse transcriptase inhibitors (NNRTIs) were tested in PHFA: Rilpivirine (ApexBio Tech LLC cat# A3765), Efavirenz (Sigma, cat# SML0536), Etravirine (ApexBio Tech LLC, cat# B2224), Delaviridine mesylate (DM) (Sigma, cat#PZ0180), Nevirapine (Nevi) (Selleckchem, cat#S1742). As a control, 3'-Azido-3'-deoxythymidine (AZT) (Sigma, cat# A2169) was used. These inhibitors were solubilized in DMSO to concentrations of 5 and 10 µg/mL, and added to PHFA seeded into 100 mm dishes at a concentration of 1.5 x 10^6 cells/dish. PHFA were inoculated with ZIKV at 0.5 pfu and treated once daily with the NNRTIs for 1 to 4 DPI, followed by whole cell lysate and RNA collection.

Immunocytochemistry. PHFA cells were seeded in two-well chamber slides, infected with ZIKV (0.1 PFU), and treated once daily with the RPV or AZT for 1 to 4 DPI. Cells were fixed with cold 4% paraformaldehyde for 20 minutes and washed three times with PBS. Cells were treated with a 5% BSA solution, followed by incubation with anti-GFAP (mouse) and anti-NS1 (rabbit) antibodies. Cells were then incubated with rhodamine and FITC-conjugated secondary antibodies, mounted with aqueous mounting medium with DAPI, and examined under immunoflourescence microscope.

Recombinant NS5 RNA polymerase preparation. Preparation of NS5 RNA polymerase was carried out with a modification of a protocol previously described[2]. The ZIKV NS5 was cloned into the pMAL™-c5X vector at the SalI and HindIII sites. MBP-NS5 expression was induced for 4 hours at 28 °C by adding isopropyl β-D-1-thiogalactopyranoside (IPTG), 0.5 mM final concentration, to *E. coli*. The cells were then harvested by centrifugation and re-suspended in 20 mM Tris-HCl pH 7.4 with 200 mM NaCl and 1 mM EDTA (amylose fast flow column buffer). Re-suspended cells were incubated on ice with lysozyme and protease inhibitor cocktail and then lysed by sonication. Clear lysates, obtained after centrifugation, were incubated overnight at 4 °C

with Amylose Resin High Flow beads (NEB). MBP-NS5 protein was then washed four times with amylose fast flow column buffer and processed to Factor Xa cleavage. MBP-NS5 fusion protein was incubated for 5 hours at room temperature in the presence of 2 mM $CaCl_2$ and Factor Xa. After centrifugation, supernatant was collected and used for NS5 activity assay. MT domain (from amino acid 1 to amino acid 264) was cloned into pMAL™-c5X vector at the SalI and BamHI sites. RdRp domain (from amino acid 265 to amino acid 903) was cloned into pMAL™-c5X vector at the EcoRI and HindIII sites. RdRp-14A was generated by substituting the corresponding amino acid residues with into alanine. RdRp-14A mutant was cloned into pMAL™-c5X vector at the EcoRI and HindIII sites using a gBlock fragment.

List of primers: NS5-full-length, F: AAGATTGTCGACGGAGGTGGGACGGGAGAGACT R: AAGATTAAGCTTTCACAACACTCCGGGTGTGGA, NS5-MTase-domain: F: AAGATTGTCGACGGAGGTGGGACGGGAGAGACT, R: AAGATTGGATCCTCATCGTGTACCCGAGCCGAG, NS5-RdRp-domain, F: AAGATTGAATTCGCTGTGGCAAGCTGTGCTG, R: AAGATTAAGCTTTCACAACACTCCGGGTGTGGA. The RdRp-14A mutant was also cloned into a mammalian expression vector (pCDNA6-myc-his-A) at HindIII-XhoI restriction enzyme sites by utilizing following primers: F: AAGATTAAGCTTATGGCTGTGGCAAGCTGTG, R: AAGATTCTCGAGCAACACTCCGGGTGTGGA.

NS5 RNA polymerase activity assay. The viral RNA polymerase NS5 ability to synthesize new viral RNA was analyzed using an *in vitro* activity assay, based on a previously described protocol[3]. One µg of ZIKV RNA and 500 ng of NS5 full-length or mutant protein (14A) with side directed mutagenesis were added to a reaction buffer containing 50 mM HEPES (pH 7.3), 0.4 mM dithiothreitol (DTT), 3 mM $MgCl_2$ and 0.4 mM of ATP, GTP, CTP and biotinylated- UTP ribonucleotides. The ribonucleotide UTP was labeled in an equimolar ratio of biotinylated-UTP and digoxigenin-UTP (DIG-UTP), for quantification of newly replicated RNA. The reaction mixtures were incubated for 1 h at 30 °C in the presence or absence of rilpivirine and

azidothymidine. The reactions were then stopped with addition of EDTA at a final concentration of 10 mM. In order to detect the incorporation of labelled UTP nucleotides, an Alpha Technology amplified luminescent proximity homogeneous assay was performed. Anti-DIG-acceptor and streptavidin-donor beads, at working concentration of 20 µg/mL, were incubated with the reaction mixture for 2 hours at room temperature in a white 96-well plate. Then, the amounts of beads bound to the DIG-labeled UTP of newly synthesized RNA could be detected by reading the plates in ALPHA compatible plate reader (Tecan). Reaction mixture without NS5 or with MBP alone was used as controls.

Mouse ZIKV infection and rilpivirine treatment. Nine IFNR knockout transgenic ($IFNR^{-/-}$) mice, obtained from Jackson laboratories, at four months were divided into three groups in two different set of experiments; 1. RPV treatment and mock infection (n=3 or n=6), 2. ZIKV infection, no treatment (n=3 or n=6), and 3. RPV treatment and ZIKV infection (n=3 or n=6). Six or twelve animals were started treatment with RPV (12.5 µg per 25 g mouse via intraperitoneal (IP) injections) two days prior ZIKV or mock infection. RPV treatments were continued daily until necropsy. Six in the first set and 12 in the second cohort of mice were infected with PRVABC59 strain of ZIKV (10^3 pfu in 20ul PBS) and three or six with a mock infection (PBS only) through footpad injections.

Mouse clinical scores and necropsy. All mice were monitored daily for survival and signs of disease as well as twice-daily weight checks and grasp test analysis. Daily physical, behavior, and motor coordination/paralysis inspections were also performed. Clinical scores were determined by grasp test and physical-behavior assessments. Mice were sacrificed based on weight loss, physical, behavior, and motor function deficits. All mice were sacrificed at the endpoint of the study at day 14 post infection. Brains were removed and half were harvested, homogenized for total RNA isolation using a commercially available kit (RNeasy mini, Qiagen). RNA samples from ZIKV-infected animals were stored at -80 °C until virus titration. The other half

of the brains were fixed in 10% neutral buffered formalin and paraffin embedded for histological examination. Organs (spleen, liver, kidney and lung) were also removed, fixed in formalin and processed for histological examination.

Histopathological Evaluation of Brain and Organ Pathology. Tissues were sectioned in a sagittal orientation at 5um for histological analysis. Slides were deparaffinized through xylene, rehydrated in graded ethanols, and stained with hematoxylin and eosin. Slides were evaluated blindly for histopathological changes (neuronal loss, gliosis, and inflammation) by a board certified veterinary anatomical pathologist (A.D.M.).

RNAscope in situ hybridization and quantitation. Zika viral RNA in the brain (frontal cortex, hippocampus, thalamus and cerebellum) and organs (spleen, liver, kidney and lung) was visualized using RNAscope in situ hybridization, according to specifications of the manufacturer (ACD Bio). Slides were deparaffinized through xylene, washed in 100% ethanol, and air-dried. Sections were treated with heat-induced target retrieval (92-100 °C) and incubated with protease (40°C). The probe was designed to target Zika viral RNA at the 866-1763 region, based off MR766 sequence (ACD Bio). The probe was hybridized in a humidity chamber at 40 °C for 2 hours. The Zika viral RNA was detected by amplification and chromogenic development using the alkaline phosphatase (AP), red chromogen detection kit (ACD Bio). Sections were counterstained with hematoxylin, dried at 60 °C and mounted. Slides were blindly imaged for quantitation of viral signal. Viral RNA was detected using Texas-Red filter fluorescence (10, 400x non-overlapping images) with a Keyence BZ-X700 Microscope. Zika viral RNA area was quantified using batch fluorescent analysis and reported as the average positive area. Zika-infected (ZIKV) Zika-infected + RPV-treated (ZIKV + RPV) groups were compared by unpaired, non-parametric t-test (Mann-Whitney), with a significance of $p<0.05$.

Dual RNAscope and immunohistochemistry. Sections were deparaffinized, rehydrated, and heat-treated with sodium citrate antigen retrieval (92-100 °C). No protease was applied to

sections. Sections were blocked with 5% levamisole in PBS for 10 minutes to block endogenous AP. Sections were hybridized with the Zika RNA probe and amplified with the AP, red chromogen kit, according to the manufacturer (ACDBio). Following verification of RNAscope detection, slides were blocked with dual endogenous enzyme block (Dako) and 10% fetal bovine serum in PBS. Sections were incubated overnight at 4 °C with antibodies against astrocytic GFAP (1:2000, ProteinTech), microglia-macrophage marker Iba1 (1:600, Wako Chemicals), T-lymphocyte marker CD3 (1:300 Dako), neuronal marker NeuN (1:500, ProteinTech), and nestin (1:300; BD Biosciences). Slides were visualized using a horseradish peroxidase (HRP)-conjugated secondary antibody and 3,3'-Diaminobenzidine chromogen (DAB)(Dako), with hematoxylin counterstain. Sections were dried at 60°C, dipped in xylene and mounted. Slides were imaged in bright-field at 200x and 600x magnification, using a Keyence BZ-X700 Microscope and accompanying software for analysis.

Statistical Analysis. All of the values presented on the graphs are given a mean ± SEM. Analysis of variance and unpaiared Student's t-test were used to analyze the statistical significance. p-values of <0.05 were considered statistically significant.

References

1. Lanciotti, R.S., et al. Genetic and serologic properties of Zika virus associated with an epidemic, Yap State, Micronesia, 2007. *Emerg. Infect. Dis.* **14**, 1232-1239 (2008).
2. Saribas, A.S., Arachea, B.T., White, M.K., Viola, R.E., Safak, M. Human polyomavirus JC small regulatory agnoprotein forms highly stable dimers and oligomers: implications for their roles in agnoprotein function.*Virology* **420,** 51-65 (2011).
3. Sacramento, C.Q, et al. The clinically approved antiviral drug sofosbuvir inhibits Zika virus replication. *Sci. Rep*. **7**, 40920 (2017).

4. Julieta Díaz-Delfín, Pere Domingo, Maria Gracia Mateo, Maria del Mar Gutierrez, Joan Carles Domingo, Marta Giralt, Francesc Villarroya. Effects of Rilpivirine on Human Adipocyte Differentiation, Gene Expression, and Release of Adipokines and Cytokines. Antimicrob Agents Chemother. 2012 Jun; 56(6): 3369–3375.

5. Barry C Johnson, Gary T Pauly, Ganesha Rai, Disha Patel, Joseph D Bauman, Heather L Baker, Kalyan Das, Joel P Schneider, David J Maloney, Eddy Arnold, Craig J Thomas, Stephen H Hughes. A comparison of the ability of rilpivirine (TMC278) and selected analogues to inhibit clinically relevant HIV-1 reverse transcriptase mutants. Retrovirology. 2012; 9: 99.

Supplemental Figures and Figure Legends

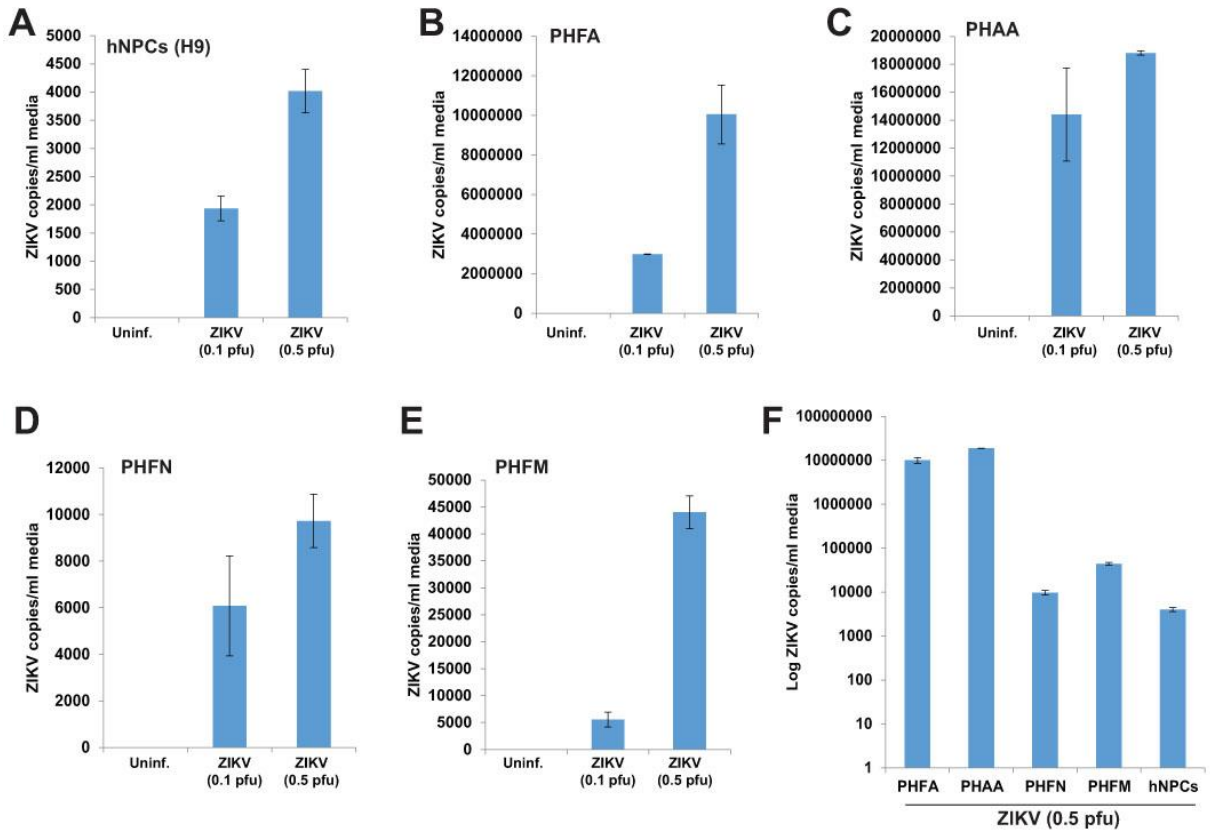

Supplemental Figure 1: ZIKV infection in primary cultures of brain cells. A. Human neuronal progenitors (NPCs-H9), **B.** Primary human fetal astrocytes (PHFA), **C.** Primary human adult astrocytes (PHAA), **D.** primary human fetal neurons (PHFN), and **E.** primary human fetal microglial cells (PHFM), were infected with 0.1 and 0.5 pfu ZIKV, and culture supernatants were analyzed by real time Q-RT-PCR at three days post-infections. ZIKV RNA copies per ml culture media were displayed as bar graphs. **F.** Log ZIKV viral loads in culture media from each cell type infected with 0.5 pfu ZIKV were displayed as bar graph.

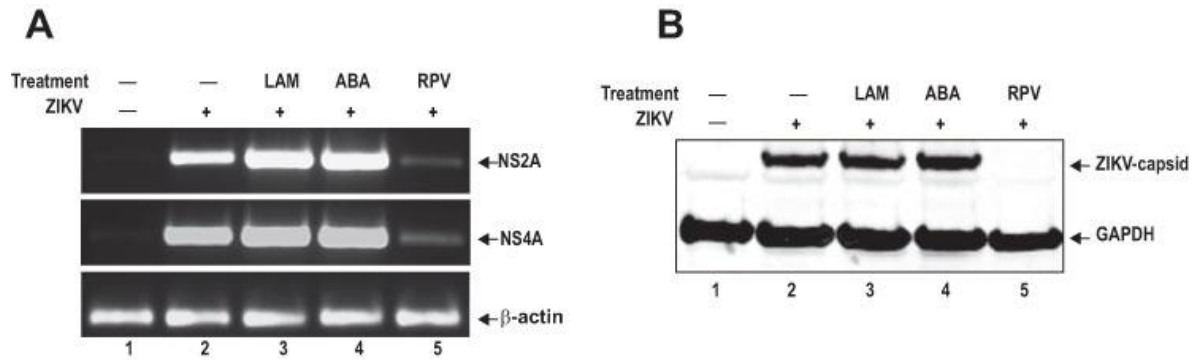

Supplemental figure 2: Effects of NNRTI on ZIKV replication in PHFA. PHFAs were infected with PRVABC59 strain of ZIKV (0.5 pfu). Cells were treated daily with LAM, ABA, and RPV (10 µg/ml). At 3 dpi, RNA lysates from cellular pellets and whole cell protein lysates were collected for analysis. A. The encoding sequence of ZIKV NS1, NS2A, and NS4A were amplified by RT-PCR in total RNA samples obtained from ZIKV infected cells, separated on a DNA agarose gel, and amplification products were visualized by ethidium bromide staining. Actin was also amplified and analyzed from the same set of samples and shown as control. B. Whole cells protein lysates from the same set of infection studies presented in panel A were processed by western blotting for the detection of ZIKV capsid protein expression by a specific antibody. GAPDH was also probed in the same membranes after stripping off the first antibody complex, and used as loading control.

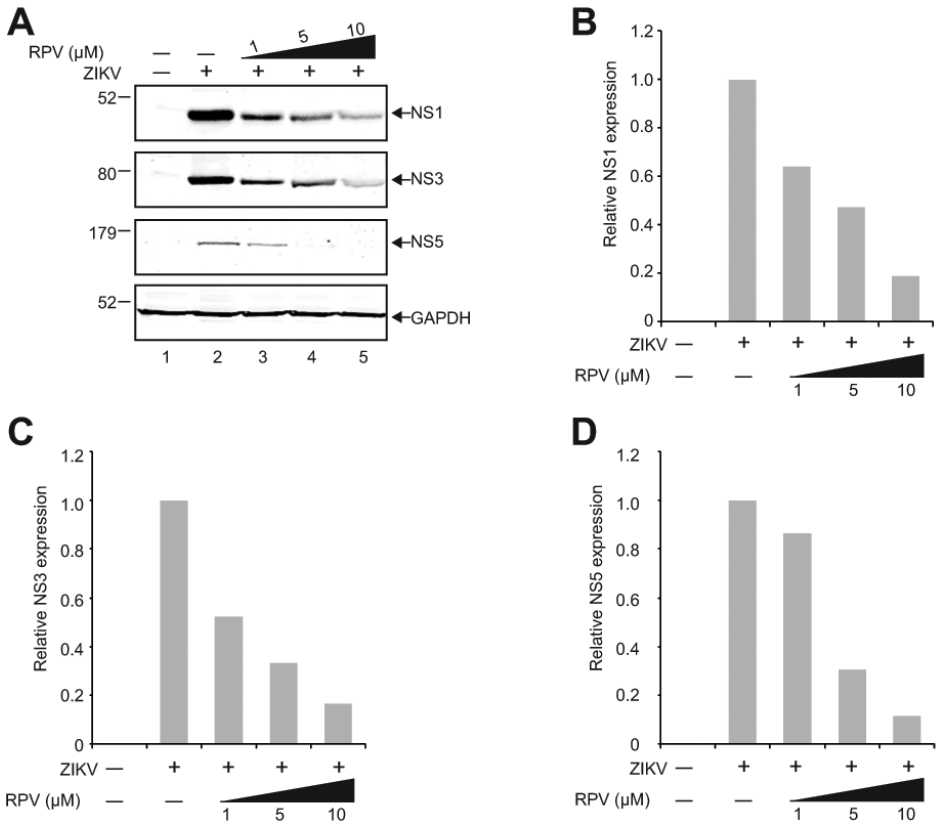

Supplemental Figure 3: Inhibition of ZIKV infection of PHFA by RPV. A. PHFA were infected with PRVABC59 strain of ZIKV (0.5 pfu) and treated with increasing concentrations of RPV (1, 5, and 10 μg/ml). Whole cell protein lysates were prepared at 4 dpi and processed by Western blotting for the detection of NS1, NS3, and NS5 protein expression. GAPDH was also probed in the same membranes after stripping off the first antibody complex, and used as loading control. **B-D.** The band intensities of NS1 (**B**), NS3 (**C**), and NS5 (**D**) shown in panel A were determined, normalized to GAPDH, and shown as bar graph as relative protein expression under each condition.

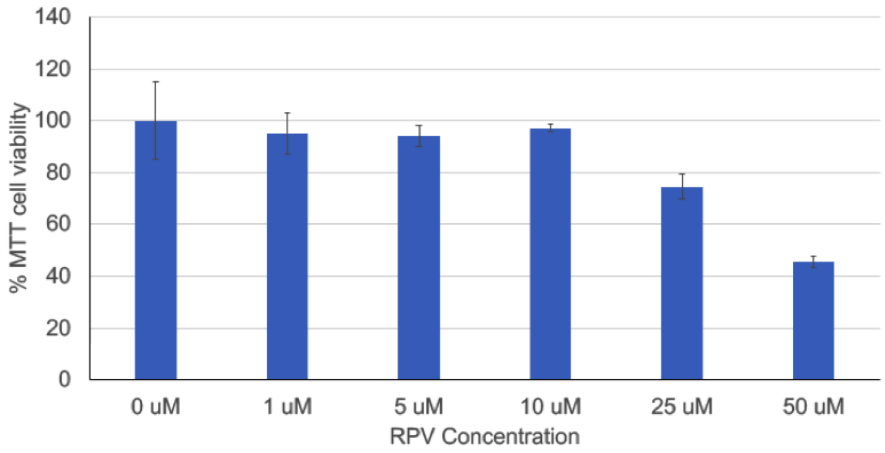

Supplemental Figure 4: Effect of RPV on viability of primary human fetal astrocytes (PHFA). PHFA cells were plated in 12 well culture dishes. Cells were treated with RPV at 0, 1, 5, 10, 25, and 50 uM concentrations. Cellular viability was assessed at 48 hr post treatments by MTT (3-(4 5-dimethylthiazol-2-yl)-2 5-diphenyltetrazolium bromide) assay. Data are mean + SEM of three independent replicates.

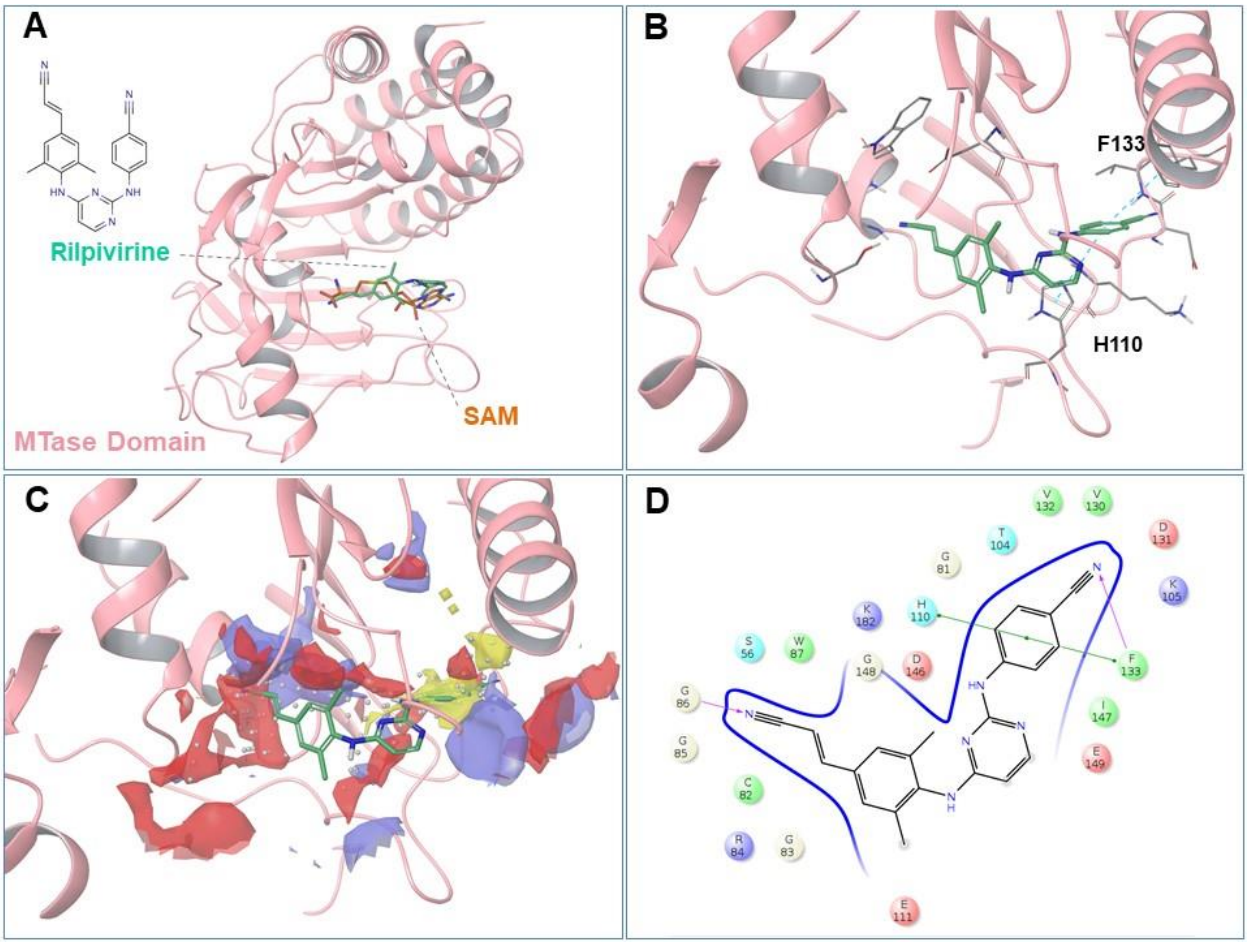

Supplemental Figure 5: Putative binding mode of RPV at the SAM site (Mtase domain). The structure of ZIKV NS5 is shown in New Cartoon representation, in pink color. A. Docking mode of RPV (green carbons) superimpose well with the crystallographic pose of the methyl donor SAH (orange carbons). B-D. Critical binding interactions are shown. In C, RPV is superimposed to complementary site map features (yellow: hydrophobic, red and blue: ligand acceptor and donor maps).

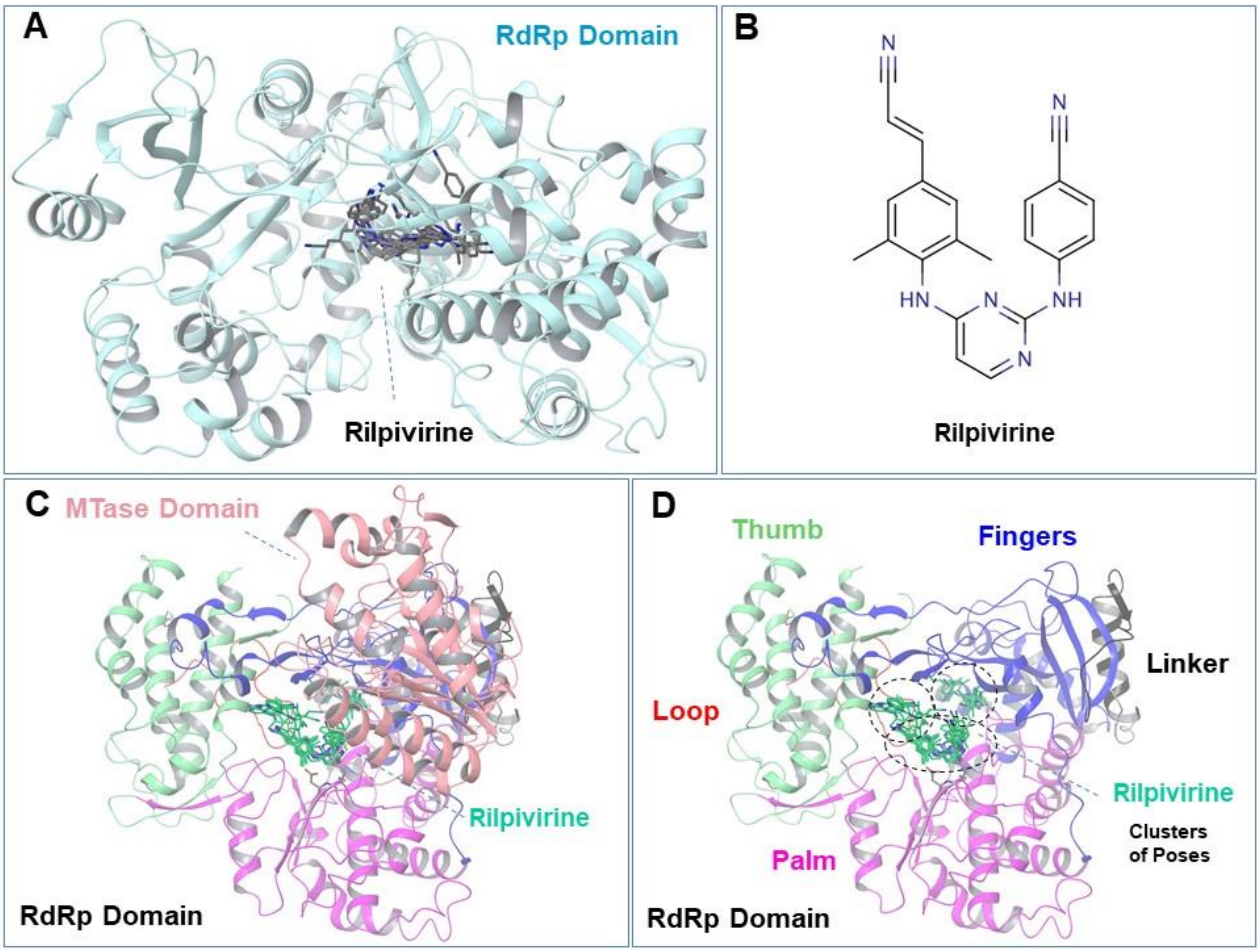

Supplemental Figure 6: Putative binding mode of RPV at the Palm Site, RdRp Domain. The structure of ZIKV NS5 is shown in New Cartoon representation, in light blue color (A) or colored according to different RdRp subdomains (finger, palm, thumb, linker and loop colored in blue, magenta, green, black and red, respectively). A-D. Docking modes of RPV (green carbons) are shown. Binding conformations of RPV at this site cluster into three distinct conformations. In A, RPV is shown in gray carbons; in C-D in green carbons. B. 2D sketch of RPV. B-D. Critical binding interactions are shown. In C, RPV is superimposed to complementary site map features (yellow: hydrophobic, red and blue: ligand acceptor and donor maps).

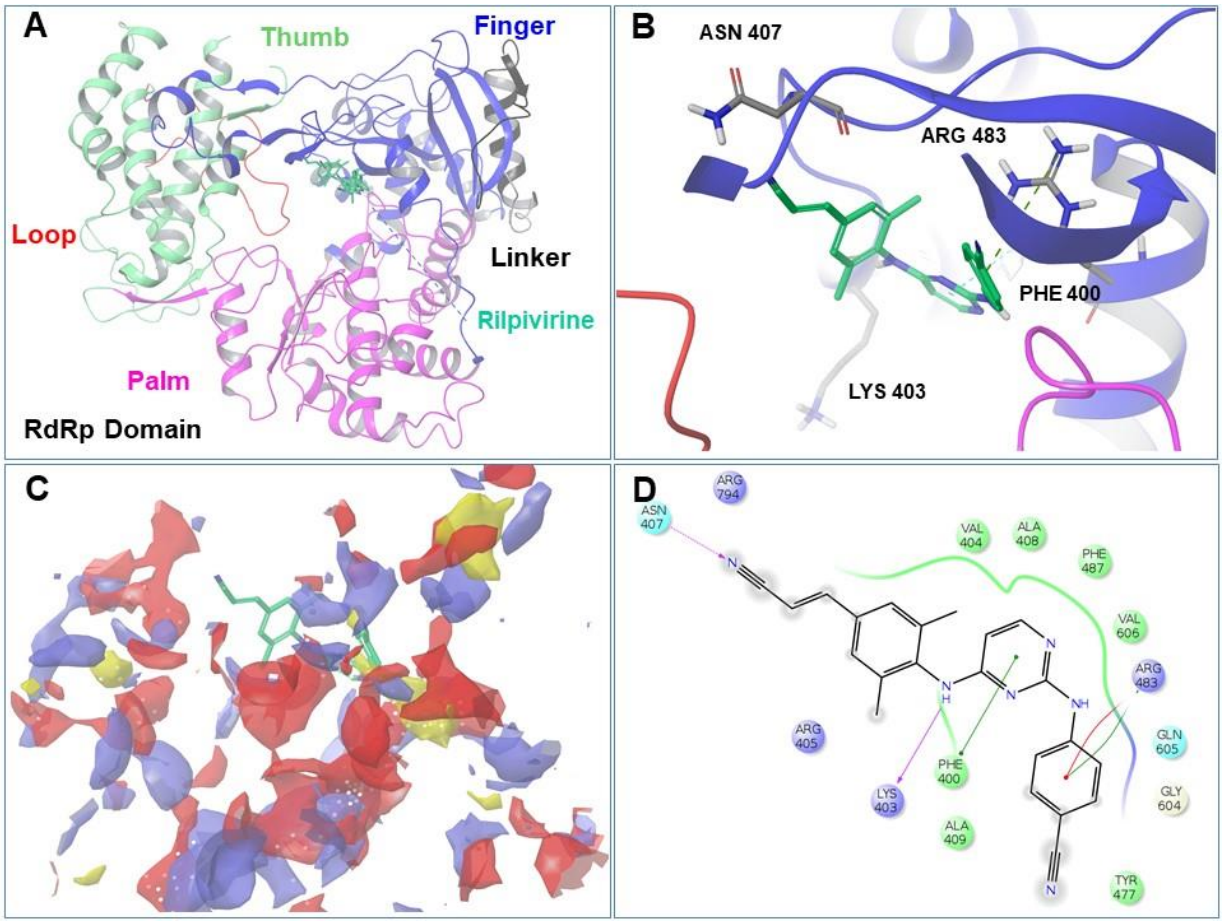

Supplemental Figure 7: Putative binding mode of RPV at the Palm Site, finger sub-domain.

The structure of ZIKV NS5 is shown in New Cartoon representation; finger, palm, thumb, linker and loop sub-domains are colored in blue, magenta, green, black and red, respectively. A. A cluster of docking modes of RPV (green carbons) is shown. B-D. Critical binding interactions are shown. In C, RPV is superimposed to complementary site map features (yellow: hydrophobic, red and blue: ligand acceptor and donor maps).

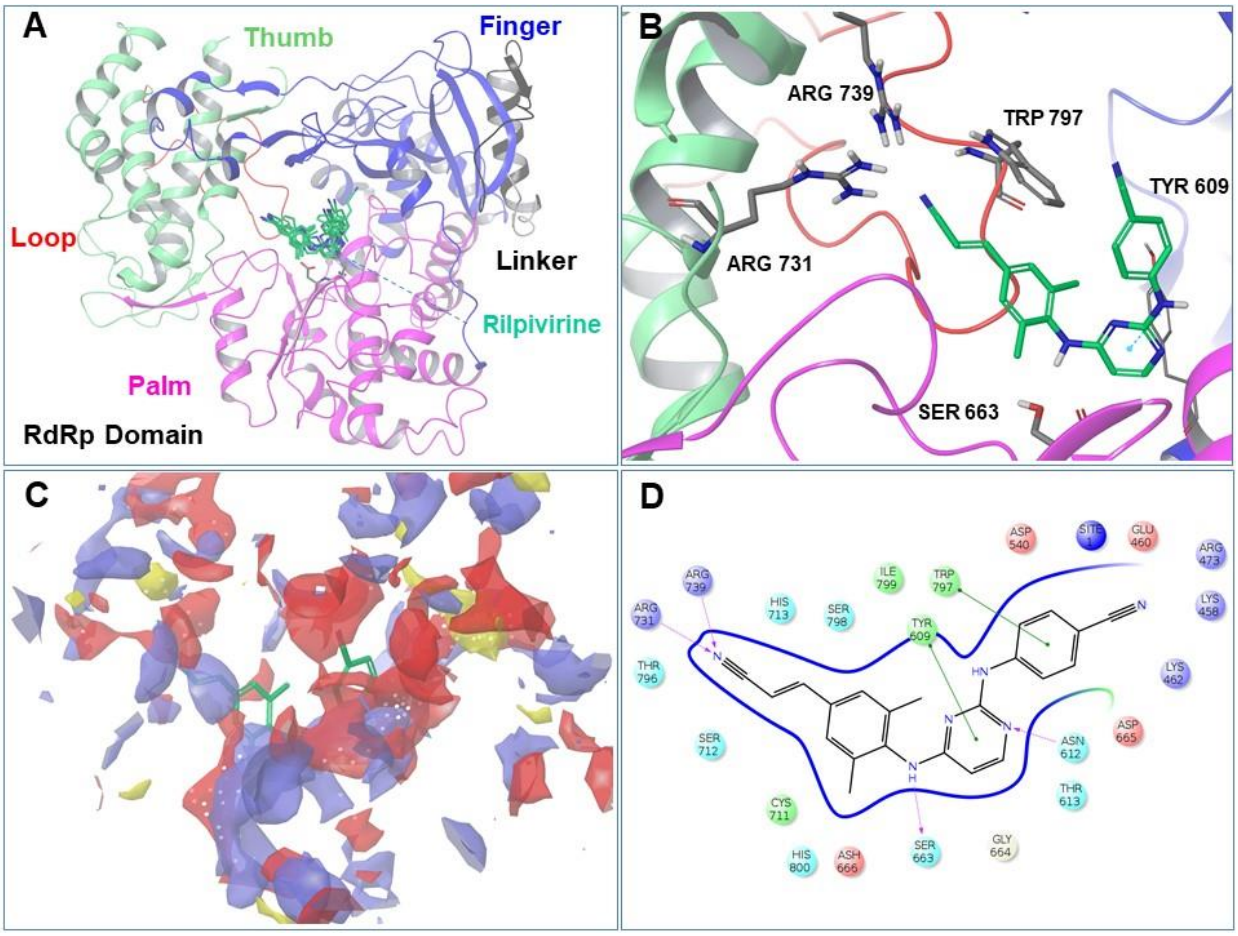

Supplemental Figure 8: Putative binding mode of RPV at the Palm Site, palm sub-domain. The structure of ZIKV NS5 is shown in New Cartoon representation; finger, palm, thumb, linker and loop sub-domains are colored in blue, magenta, green, black and red, respectively. A. A cluster of docking modes of RPV (green carbons) is shown. B-D. Critical binding interactions are shown. In C, RPV is superimposed to complementary site map features (yellow: hydrophobic, red and blue: ligand acceptor and donor maps).

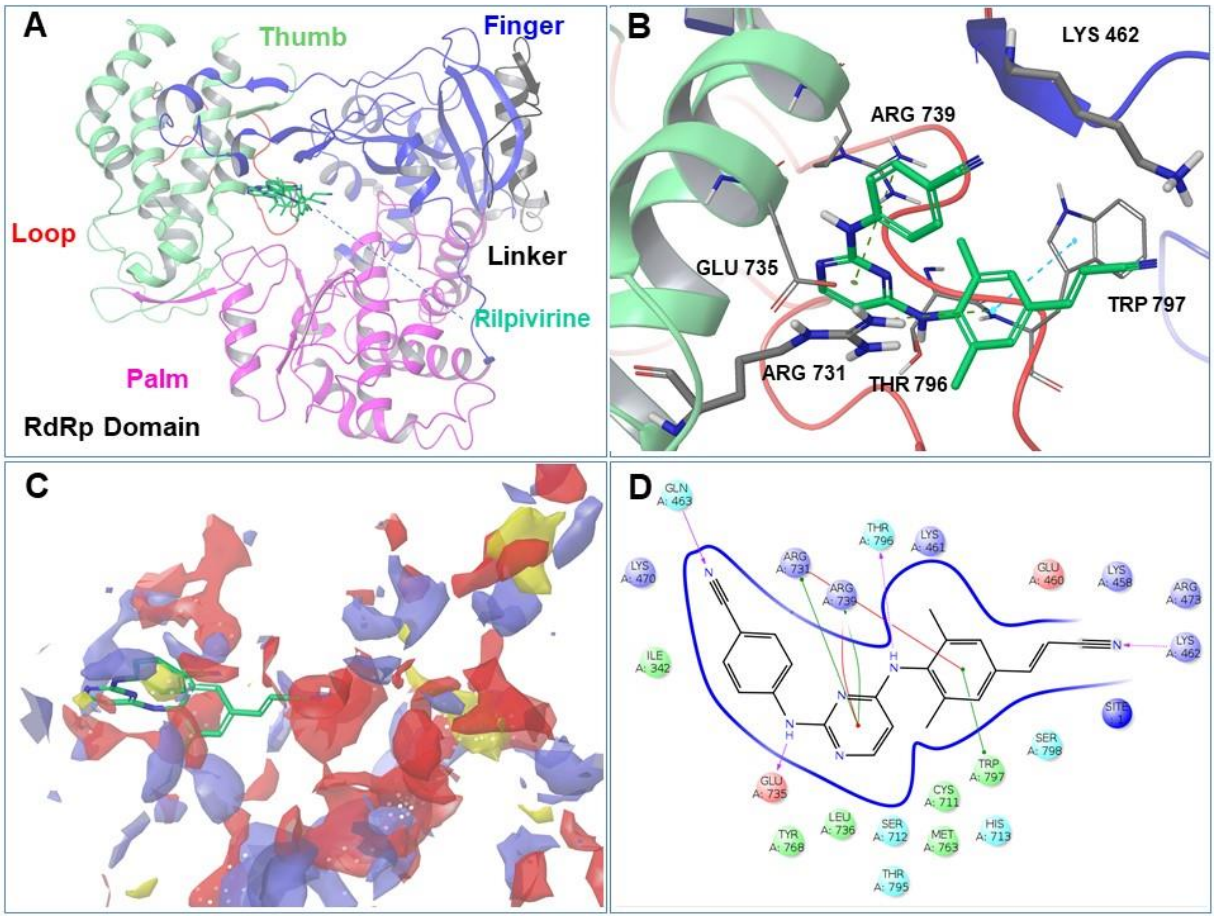

Supplemental Figure 9: Putative binding mode of RPV at the Palm Site, thumb sub-domain. The structure of ZIKV NS5 is shown in New Cartoon representation; finger, palm, thumb, linker and loop sub-domains are colored in blue, magenta, green, black and red, respectively. A. A cluster of docking modes of RPV (green carbons) is shown. B-D. Critical binding interactions are shown. In C, RPV is superimposed to complementary site map features (yellow: hydrophobic, red and blue: ligand acceptor and donor maps).

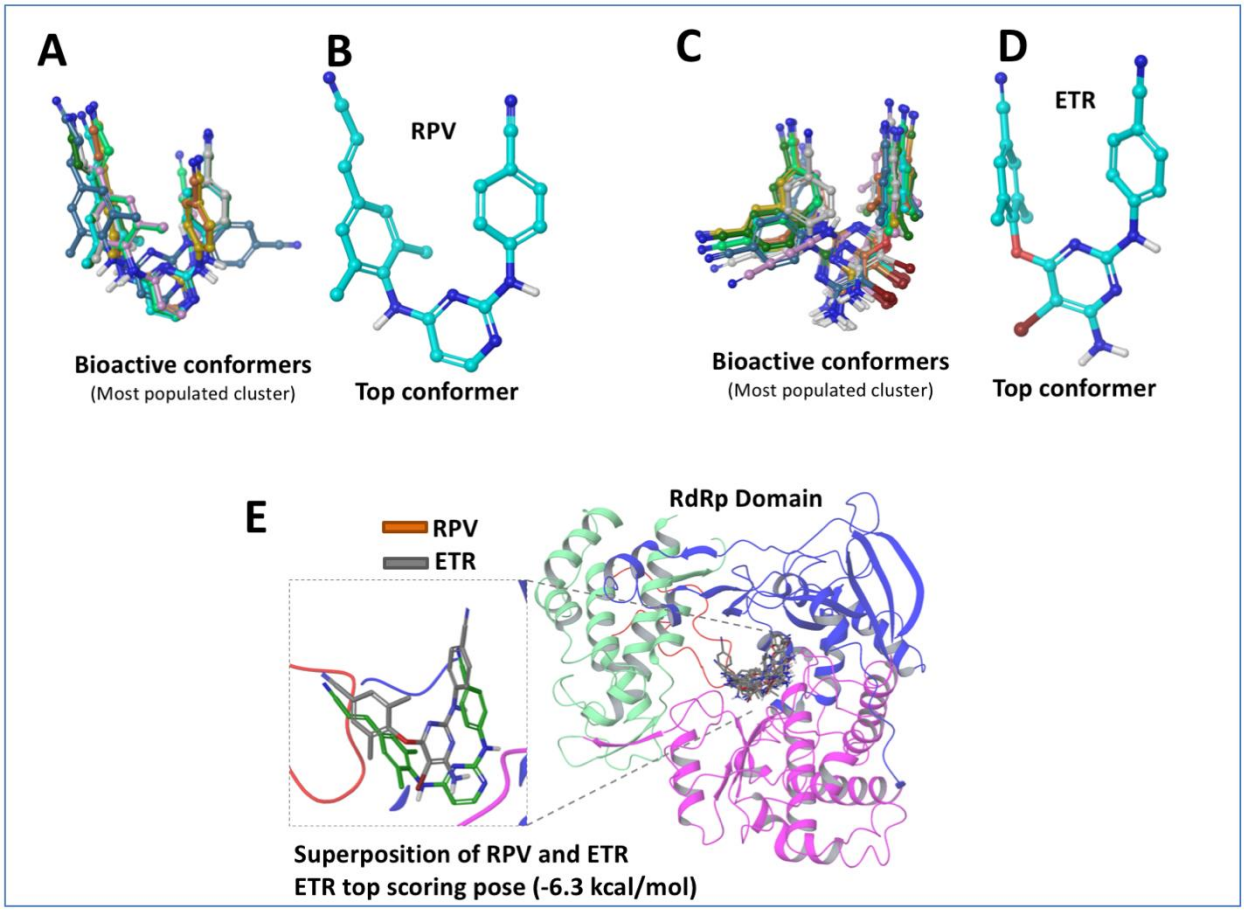

Supplemental Figure 10: Bioactive conformation and best predicted binding of RPV to the RdRp Domain of NS5. Most populated cluster of conformers of RPV (A) and top conformer (B). Bioactive conformation and predicted binding of ETR to the RdRp Domain of NS5 (compared to RPV). Most populated cluster of conformers of ETR (C) and top conformer (D). Binding mode of ETR to the NS5 RdRp domain (E), generated by molecular docking, is compared a representative binding mode of RPV. In all cases, both ETR and RPV adopts the “horseshoe” binding conformation that was previously observed in the experimental complex of RPV bound to HIV-1 RT (*).

(*) Das, K. et al. High-resolution structures of HIV-1 reverse transcriptase/TMC278 complexes: Strategic flexibility explains potency against resistance mutations. Proc. Natl. Acad. Sci. 105, 1466 (2008).

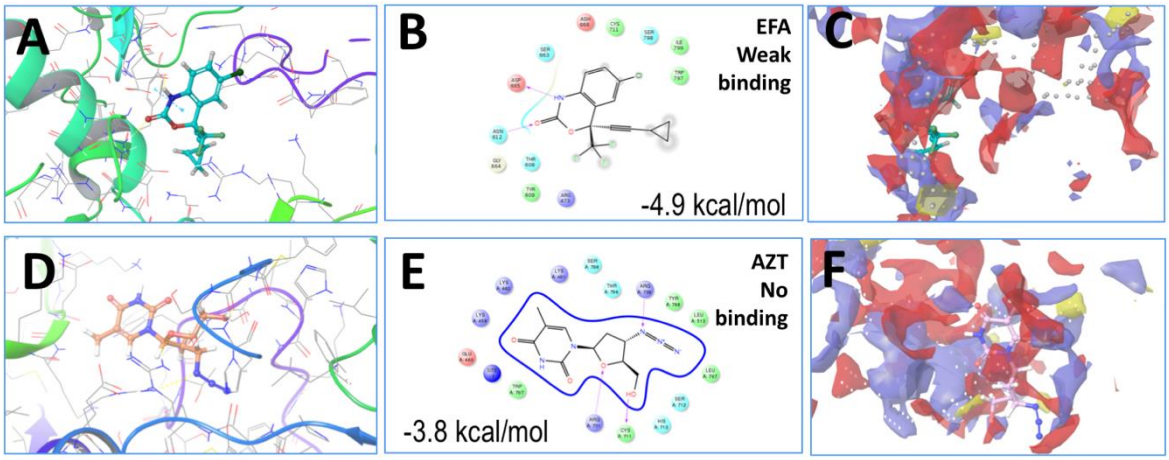

Supplemental Figure 11: Predicted binding modes of the NNRTI EFA and the NRTI AZT to the RdRp domain of NS5. Docking scores are indicated in parenthesis and correlate with experimental data showing that, while the inhibitory effect of EFA could only be detected at high concentrations (suggesting weak binding), AZT did not interfere at all (suggesting no binding) with NS5 activity (Fig. 2, panels B and D).

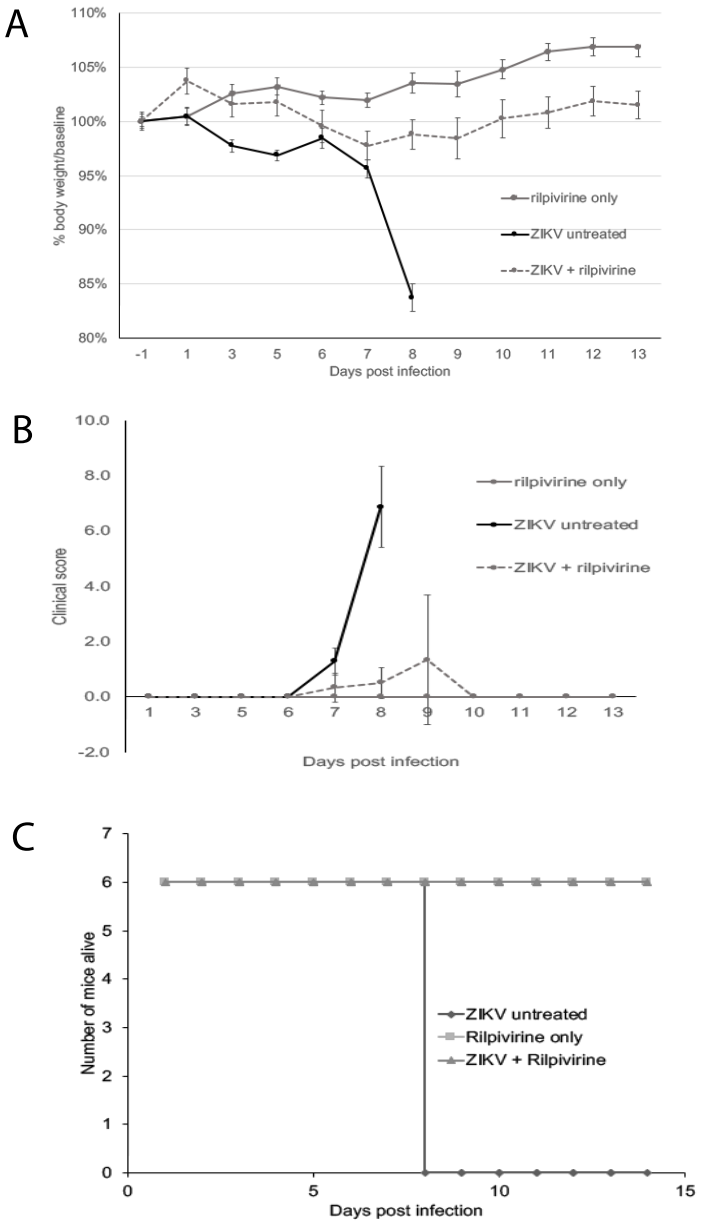

Supplemental Figure 12: RPV reverses the mortality and decreases the viral burden in the IFNR$^{-/-}$ mice. Eighteen IFNR knockout transgenic (IFNR$^{-/-}$) mice, obtained from Jackson laboratories, at four months were divided into three groups; 1. RPV treatment and mock infection (n=6), 2. ZIKV infection, no treatment (n=6), and 3. RPV treatment and ZIKV infection (n=6).

twelve animals were started treatment with RPV two days prior ZIKV or mock infection. RPV treatments were continued daily. Twelve mice were infected with PRVABC59 strain of ZIKV and six with a mock infection (PBS only) through footpad injections. **A.** Body weights were measured for each mouse from the three groups (closed square-rilpivirine only; closed circle- ZIKV untreated; open triangle- ZIKV + RPV) until the end of the study (14 days post infection (dpi)). Data are shown as a percent of body weight compared to baseline. **B.** Grasp tests were performed daily starting at 4 dpi and analyzed for clinical scoring for the three groups. **C.** Survivor curve analysis is shown based on the Kaplan-Meier estimates. All animals in the RPV only and ZIKV + RPV groups survived until the end of the study. The ZIKV mice were sacrificed at 8 dpi.

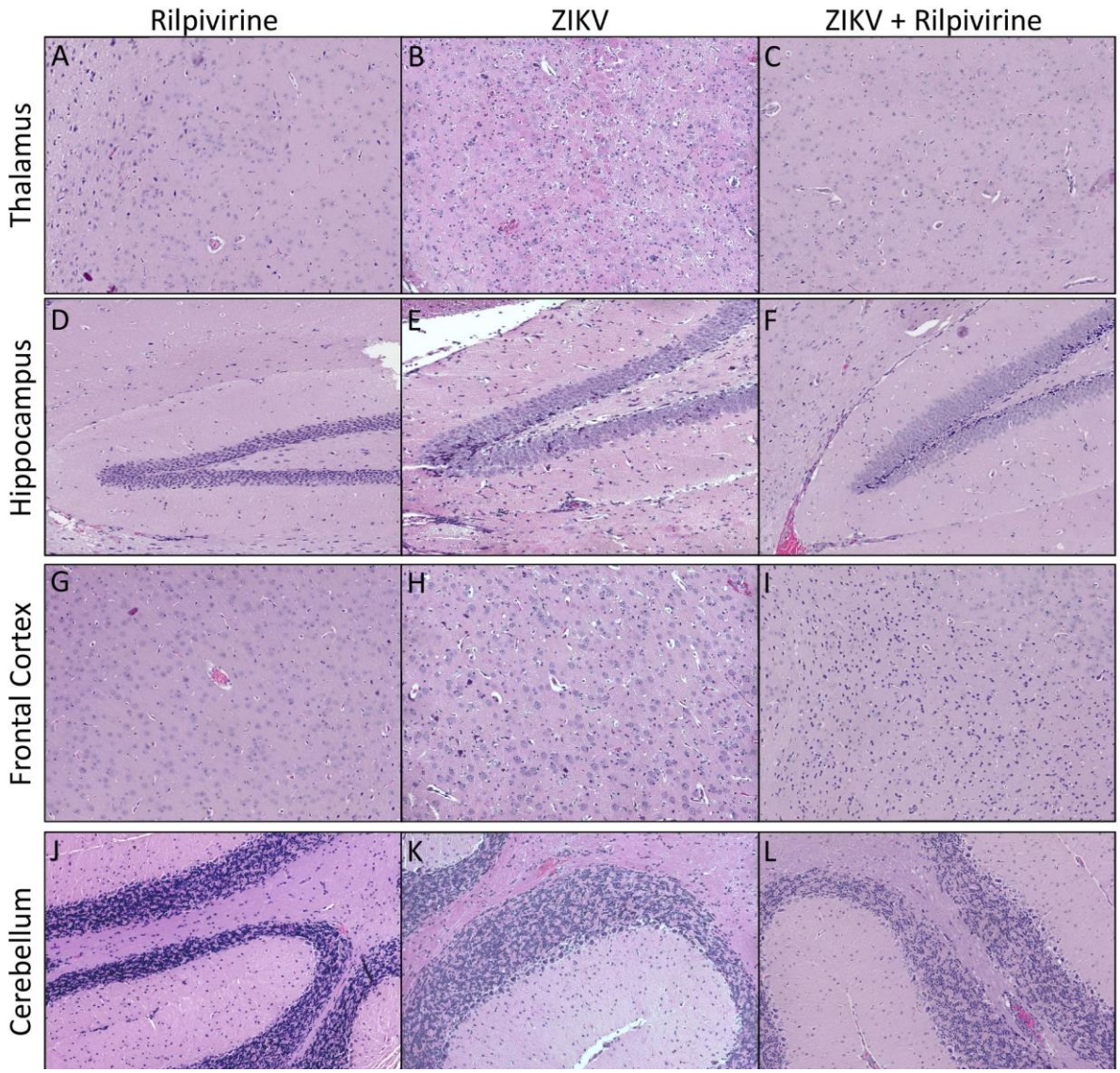

Supplemental Figure 13: Significant inflammation and necrosis with ZIKV in the brains of IFNR$^{-/-}$ infected mice. Thalamus (**A-C**), hippocampus (**D-F**), frontal cortex (**G-I**) and cerebellum (**J-L**) from RPV only (RPV) **(A, D, G, J)**, ZIKV-infected animals (ZIKV) **(B, E, H, K)** and ZIKV - infected, RPV-treated animals (ZIKV + RPV) **(C, F, I, L)** were stained with hematoxylin and eosin. **(A, D, G, J)**. The rilpivirine-only control brains were unremarkable. **(B, E, H, K)**. All brain regions (thalamus, hippocampus, frontal cortex and cerebellum) examined in the ZIKV only mice had significant inflammation, but also abundant apoptotic/necrotic cell damage. **(C, F, I, L)**. In the RPV

treated ZIKV infected animals, there was still significant inflammation, but no apoptotic/necrotic cell damage was seen.

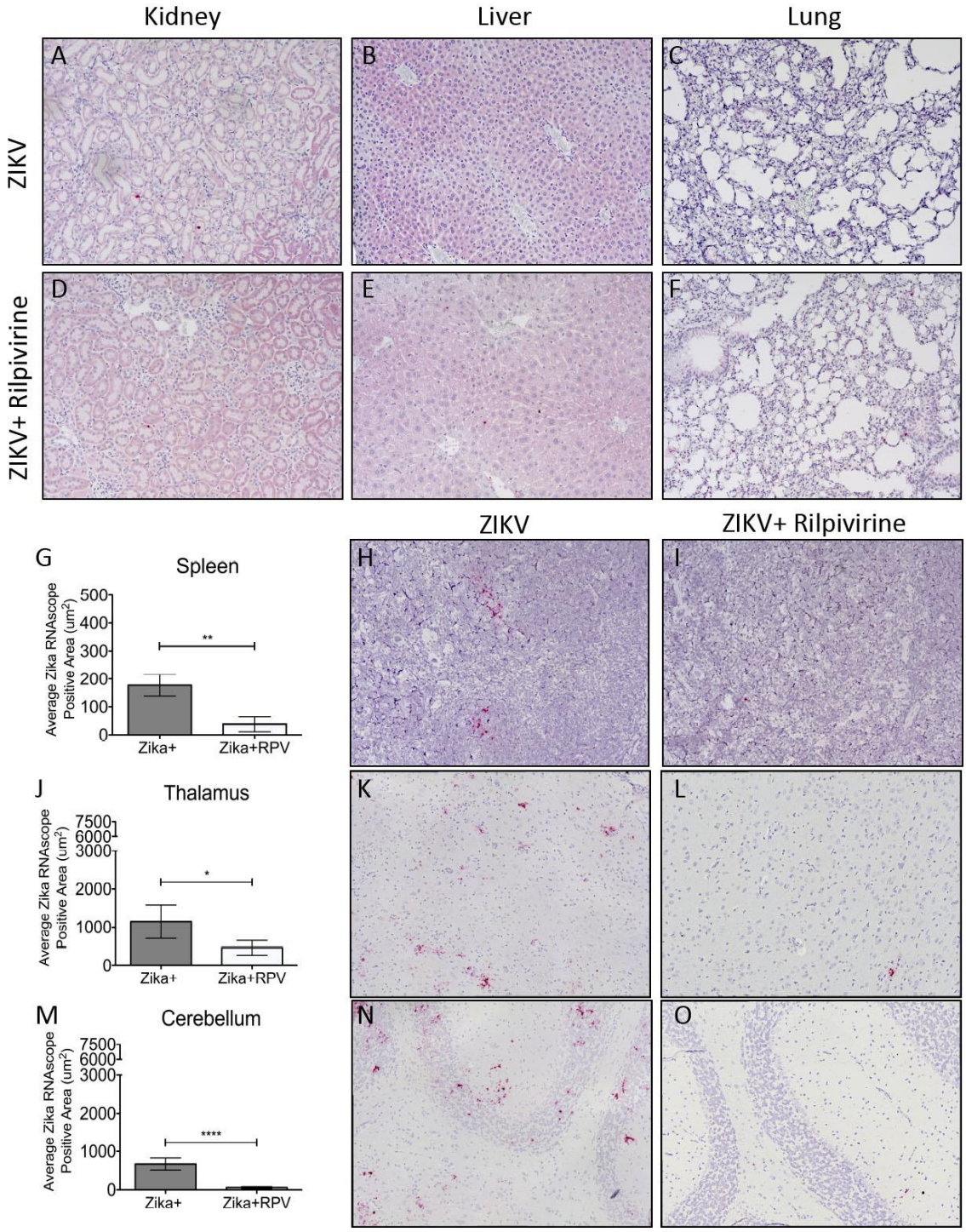

Supplemental Figure 14: Comparison of ZIKV RNA in kidney, liver, lungs, spleen, thalamus and cerebellum. ZIKV RNA was visualized with RNAscope (red) in kidney **(A-B)**, liver **(C-D)**, and lungs **(E-F)** of ZIKV-infected animals (ZIKV) and ZIKV -infected, RPV-treated animals (ZIKV

+ RPV). **(G)** Quantitation of ZIKV RNA in spleen showed low levels of ZIKV RNA in the ZIKV infected animals (176.8 ± 39.1 μm^2), which significantly decreased with RPV treatment (38.0 ± 26.7 μm^2) (P<.001). **(H)** Representative image of a spleen ZIKV RNAScope in situ reveals high viral RNA signal in ZIKV mice. **(I)** Representative image of spleen ZIKV RNAScope staining shows few ZIKV RNA+ cells in ZIKV + RPV mice. **(J)** Quantitation of ZIKV RNA in thalamus showed moderate levels of ZIKV RNA in the ZIKV infected animals (1149.3 ± 440.7 μm^2), which significantly decreased with RPV treatment (464.8 ± 193.5μm^2) (P<.05). **(K**) Representative image of a thalamus ZIKV RNAScope in situ reveals moderate viral RNA signal in ZIKV mice. **(L)** Representative image of thalamus ZIKV RNAScope staining shows decreased ZIKV RNA+ cells in ZIKV + RPV mice. **(M)** Quantitation of ZIKV RNA in cerebellum showed moderate levels of ZIKV RNA in the ZIKV infected animals (669.9 ± 157.9 μm^2), which significantly decreased with RPV treatment (56.4 ± 25.0 μm^2) (P<.05). **(N)** Representative image of a cerebellum ZIKV RNAScope in situ reveals moderate viral RNA signal in ZIKV mice. **(O)** Representative image of cerebellum ZIKV RNAScope staining shows decreased ZIKV RNA+ cells in ZIKV + RPV mice. The average Zika RNA signal area was quantitated as the average of 10, non-overlapping 40X images from each animal (n=3/group), using a Keyence BZ-X700 microscope. Bar graphs show average Zika RNA area (mean, SEM). Comparison of means was determined by Mann-Whitney, two-tailed t-test. (*P<0.05, ****P<0.0001)